Journal of Fluids and Structures 119 (2023) 103875

Contents lists available at ScienceDirect

Journal of Fluids and Structures

journal homepage: www.elsevier.com/locate/jfs

Validation of a control-oriented point vortex model for a cyclorotor-based wave energy device☆

Andrei Ermakov [a,*], Florent Thiebaut [b], Grégory S. Payne [b,1], John V. Ringwood [a]

[a] The Centre for Ocean Energy Research, Maynooth University, Maynooth, W23 F2H6, Co. Kildare, Ireland
[b] Ecole Centrale de Nantes, 1 rue de la Noë, Nantes, 44300, France

ARTICLE INFO

Article history:
Received 1 January 2023
Received in revised form 16 February 2023
Accepted 16 March 2023
Available online xxxx

Keywords:
Cyclorotor
Model validation
Wave energy converters
LiftWEC
Hydrofoils
Experimental results

ABSTRACT

Recently conducted analytical assessment of the potential performance of cyclorotor wave energy converters (WECs) have shown that such devices offer the best wave absorption behaviour, if energy capture can be optimised through suitable control. Such claims require additional investigation. This article is dedicated to validation of the control-oriented point vortex model of cyclorotor WECs against numerical and experimental assessments conducted by various research groups. The validation is conducted in terms of the traditional metrics for cyclorotor WECs: (a) cancellation of incoming waves; (b) generation of lift and drag forces (c) mechanical power generation.

It is shown that the point vortex model generally confirms the previously conducted analytical assessment of device performance. However, accounting for the influence of the hydrofoil induced wakes decreases performance estimates to some extent. It is also shown that, overall, wave cancellation metrics are more optimistic than actual shaft power generation.

Analysis of the lift and drag coefficients, which were derived from experimental data, reveal a range of hydrodynamic and mechanic effects which could influence actual device performance. It has been shown that, due to the complexity of hydrodynamic effects, lift and drag coefficients for the control-oriented model should be considered not only as functions of the Reynolds number and angle of attack, but also related to submergence of the foils and direction of their rotation with respect to the free surface. This method allows us to achieve the best validation against experimental results in terms of generation of tangential and radial forces.

1. Introduction

Lift force oriented cyclorotor-based wave energy converters (WECs) (Folley and Whittaker, 2019; Ermakov and Ringwood, 2021c) can be an alternative to traditional wave energy extraction methods based on buoyancy or diffraction forces (Guo and Ringwood, 2021). This relatively new technology has started to attract increasingly more attention from various research groups (Atargis Energy Corporation, 2022; LiftWEC Consortium, 2022; Yu et al., 2021; Wu and Zuo, 2022). The propagation of water waves causes circulation of water particles which can generate significant lift forces on hydrofoils.

☆ This project has received funding from the European Union's Horizon 2020 research and innovation programme under grant agreement No. 851885. The authors are grateful for the support of the Irish Centre for High-End Computing (ICHEC).

* Corresponding author.
E-mail address: andrei.ermakov@mu.ie (A. Ermakov).
1 Present address: Farwind Energy, 1 rue de la Noë, 44300, Nantes, France.

https://doi.org/10.1016/j.jfluidstructs.2023.103875

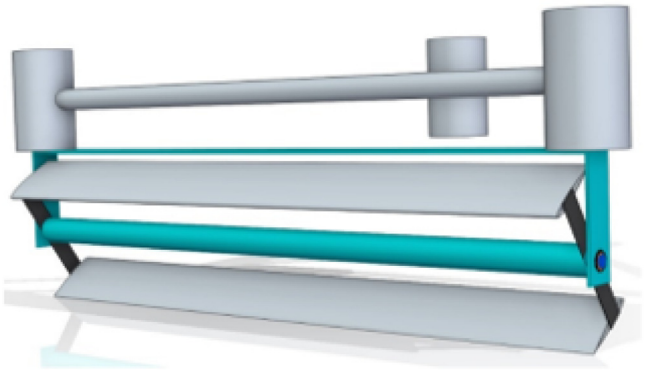

Fig. 1. The LiftWEC cyclorotor-based wave energy converter concept (LiftWEC Consortium, 2022; Fernandez Chozas et al., 2021).

The cyclorotor hydrofoils (Fig. 1) can be made to follow water particle circulation, thus maintaining the optimal angle of attack. The tangential component of the lift force generates a torque on the cyclorotor shaft, which provides direct (unidirectional) input to the electricity generator. However, as has been shown in Siegel (2019), Ermakov et al. (2022a) and Ringwood and Ermakov (2022), the performance of the cyclorotor depends heavily on the action of an optimal real-time control strategy. Optimal control of the rotational rate, and hydrofoil pitch angle, can triple the generated power, as well as mitigating the significant hydrodynamic loads encountered (Ermakov et al., 2022a; Ringwood and Ermakov, 2022; Arredondo-Galeana et al., 2023a).

The most recent performance assessment conducted by the Atargis Energy Corporation (2022), for their concept of a cyclorotor with two hydrofoils (CycWEC), estimates electricity production at 3000 MW/h for regular, and 1800 MW/h for irregular, waves (Chitale et al., 2021). The CycWEC was also identified as having the highest electrical energy production (∼40%) and power load factor (∼45%) for the Galician coast (NW Spain), in contrast to traditional WECs, in simulations conducted in Arguilé-Pérez et al. (2022).

Other recent performance estimates have been determined within the LiftWEC consortium (LiftWEC Consortium, 2022), which is a collaboration of 10 European universities and industry partners. The LiftWEC concept represents a cyclorotor with two hydrofoils attached to a spar buoy (Fig. 1). It has been noted that, while the LCoE of traditional WECs is expected to be ∼200 €/MWh by 2025 (Têtu and Fernandez Chozas, 2021), a recent optimistic LCoE estimate for a cyclorotor-based LiftWEC with technology readiness level (TRL) 4 is ∼140 €/MWh (LiftWEC Consortium, 2022). Such an appealing number is justified by the similarity to offshore wind and 'propeller based' technology (Martinez and Iglesias, 2022). The LiftWEC device can be also considered complimentary to wind, with possible installation on existing floating offshore wind platforms.

However, the recent (Siegel, 2019; LiftWEC Consortium, 2022) and older (Hermans et al., 1990; Scharmann, 2018) performance estimates were obtained with the use of different analytical and numerical models, using a variety of performance metrics. The models were validated against different experiments which targeted different goals, such as wave generation and cancellation (Hermans et al., 1990; Siegel et al., 2012a), or maximisation and stabilisation of mechanical torque (Scharmann, 2018; LiftWEC Consortium, 2022). The current level of development of cyclorotor-based wave energy technology requires the establishment of a single, common analytical model which can reproduce and explain all the previous experimental and analytical results. The model should be relatively simple and suitable for control design and performance assessment. The authors propose the use of the developed point vortex model (Ermakov and Ringwood, 2021a,b, 2022) for this purpose.

In Section 2, the authors present a review of models and metrics for cyclorotor-based WEC prototypes, which were used by previous researchers. Section 3 is dedicated to the control-oriented point vortex model, documenting the assumptions, limitations, and relationship to previous metrics. In Section 4, the authors attempt to reproduce the Atargis CycWEC (Siegel, 2019) performance assessment, using the point vortex model, and compare the results for wave cancellation and mechanical power generation metrics. In Section 5, the authors analyse the most recent experimental test of a 2D LiftWEC prototype (Thiebaut et al., 2021; Thiebaut and Payne, 2021a), derive lift and drag coefficients, and validate a point vortex model in terms of generation of tangential and radial forces. The Conclusions (Section 6) are dedicated to the discussion of the applicability of the point vortex model to performance assessment and control design.

2. Review of models and validation metrics for cyclorotor-based WEC prototypes

2.1. Wave radiation and cancellation

The original metric, proposed for analytical model validation and performance evaluation for a cyclorotor WEC, is based on the assessment of waves radiated by the rotating device. Such a metric was used during tests of the first

cyclorotor-based WEC concept — 'the Rotating Foil' in 1990 (Hermans et al., 1990; Hermans and Pinkster, 2007). The tests were conducted in the deep-water basin of the Maritime Research Institute deep-water basin, in the Netherlands. The experimental setup consisted of a single hydrofoil which was actively rotated in still water and radiated waves. The experimenters adjusted the rotational velocity and hydrofoil pitch angle and studied the amplitudes and periods of the generated waves. It was shown that the period of the generated waves was equal to the period of rotation of the foil, while the wave amplitude was proportional to the fluid circulation Γ caused by the moving hydrofoil.

The authors proposed to model the hydrofoil, and generated waves, by using the complex potential which describes the motion of a point vortex under a free surface (Wehausen and Laitone, 1960):

$$\mathcal{F}(z,t) = \frac{\Gamma(t)}{2\pi\,\mathrm{i}} Log\left[\frac{z-c(t)}{z-\tilde{c}(t)}\right] + \frac{g}{\pi\,\mathrm{i}}\int_0^t\int_0^\infty \frac{\Gamma(\tau)}{\sqrt{gk}} e^{-\mathrm{i}k\left(z-\tilde{c}(\tau)\right)} \sin\left(\sqrt{gk}(t-\tau)\right) dk d\tau \tag{1}$$

where $c(t) = x(t) + \mathrm{i}y(t)$ is the position of the hydrofoil, $\tilde{c}(t)$ is the complex conjugate of $c(t)$, g is the acceleration due to gravity, k is the wave number, τ is the dynamic time parameter, and $\Gamma(t)$ is the circulation of the vortex.

It is assumed that the intensity of circulation of the vortex Γ is proportional to the lift force F_L generated on the foil, in accordance with the Kutta–Joukowski theorem (Batchelor, 1967):

$$\Gamma = F_L/(\rho|\hat{V}|) = \frac{1}{2} C_L(\alpha)\,|\hat{V}|\,C \tag{2}$$

where F_L is the lift force, ρ is the water density, $\hat{V}$ is the relative foil/fluid velocity, C_L is the lift coefficient, α is the angle of attack, and C is the length of the foil chord.

Then, the velocity potential Φ_H can be found as:

$$\Phi_H(x,y) = Re[\mathcal{F}(z,t)] \tag{3}$$

and the free surface perturbation η_{h_i} caused by the rotating underwater vortex can be calculated from the dynamic boundary condition:

$$\eta_{h_i} = -\frac{1}{g}\left(\frac{\partial \Phi_{H_i}}{\partial t}\right)_{y=0} \tag{4}$$

The results, presented by researchers in Hermans et al. (1990) and Hermans and Pinkster (2007), show successful validation of the developed analytical model against experimental results. The experimentally measured amplitudes, and periods of radiated waves, are very close to the analytical results.

The developed mathematical model, supported by experimental results, formed a strong foundation for future research of the technology and inspired the foundation of the Atargis Energy Corporation by Stefan Siegel (Atargis Energy Corporation, 2022). Atargis proposed a two-hydrofoil cyclorotor — the Cycloidal Wave Energy Converter (CycWEC). This cyclorotor configuration allows it to generate waves with equal amplitude for wave crest and trough, making the radiated waves very close to monochromatic waves. The proposed operational principle of the device is the cancellation of incoming waves. It was shown analytically, and experimentally (Siegel et al., 2012a,b; Fagley et al., 2012; Siegel, 2013), that a cyclorotor can entirely cancel the incoming (close to monochromatic) waves by generating waves with the same amplitude and period, but with opposite phase. The conducted experiments include tests of a 2D CycWEC 1:300 prototype in the US Air Force Academy (Siegel et al., 2012a,b) in 2011, and a 3D 1:10 prototype in a wave tank at the Texas A&M Offshore Technology Research Centre (Fagley et al., 2012; Siegel, 2013) in 2012. The wave cancellation effect has also been reproduced in a two dimensional Ansys CFD model, presented in the master thesis of Caskey, C (Caskey, 2014).

The most recent publications from Atargis are dedicated to analytical estimation of the potential performance of the proposed device, in terms of power of radiated/cancelled waves (Siegel, 2014, 2019). According to these wave cancellation metrics, the wave power changes can be evaluated via up-wave and down-wave free surface perturbations at the gauge points within the rotational period T. Three types of waves are considered: incoming waves, transmitted waves and waves radiated upstream from the rotor.

As an example of the incoming wave, we consider the velocity potential for monochromatic Airy waves:

$$\Phi_W = \frac{Hg}{2\omega} e^{ky} \sin(kx - \omega t + \phi) \tag{5}$$

where H is the wave height, ω is the wave frequency, k is the wave number, and ϕ is the relative wave phase.

The free surface perturbation, caused by incoming waves, can be found as:

$$\eta_{incoming-wave} = -\frac{1}{g}\left(\frac{\partial \Phi_W}{\partial t}\right)_{y=0,\,x=-\lambda} \tag{6}$$

while the overall free surface elevation, at the gauge point located down-wave, at $x = \lambda$, can be evaluated as the sum:

$$\eta_{down-wave} = -\frac{1}{g}\left(\frac{\partial(\Phi_W + \Phi_{H_1} + \Phi_{H_2})}{\partial t}\right)_{y=0,\,x=\lambda} \tag{7}$$

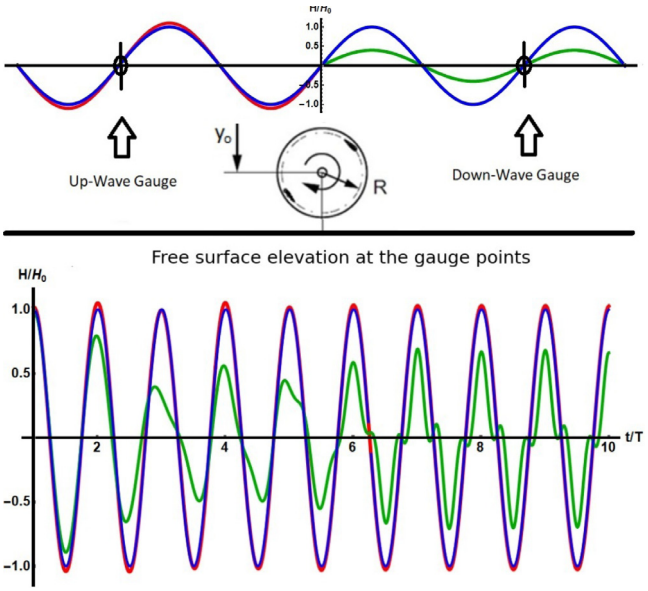

Fig. 2. The wave cancellation effect for the CycWEC (Siegel, 2019) cyclorotor, with $\gamma_1 = -\gamma_2 = 11°$, which rotates in monochromatic waves $T = 10$ s, $H_0 = 2$ m. The blue line represents the original incoming wave, while the red and green lines show the actual up-wave and down-wave free surface elevation measured at the gauge points located at a $\pm$ wave length distance. (For interpretation of the references to colour in this figure legend, the reader is referred to the web version of this article.)

Finally, the profile of the waves radiated up-wave from the rotor, at the point $x = -\lambda$, can be found using the equation:

$$\eta_{up-wave} = -\frac{1}{g}\left(\frac{\partial(\Phi_{H_1} + \Phi_{H_2})}{\partial t}\right)_{y=0,\, x=-\lambda} \tag{8}$$

It is shown in Ermakov et al. (2022a,b) that, after approximately eight wave periods, the system variables become stable, and the mechanical and hydrodynamic effects became periodic (see Fig. 2). At this stage, a spectral analysis can be conducted to determine the frequency of the waves passing through the gauge points within the time period T. According to Siegel (2019, 2014), the first harmonic of the wave profile, evaluated down-wave (7), corresponds to the partially cancelled incoming wave or transmitted wave, while all other harmonics correspond to the waves radiated down-wave from the cyclorotor. The profile of the waves radiated up-wave can be obtained using (8), and their amplitudes can be calculated using spectral analysis.

Thus, the power which is available for WEC absorption, can be obtained as:

$$P_{Wave} = P_{Incident} - P_{Transmitted} - P_{Radiated} \tag{9}$$

The wave cancellation metric also traditionally (Siegel, 2019) includes power losses due to drag P_{Drag}:

$$P_{Cancelled} = P_{Wave} - P_{Drag} \tag{10}$$

2.2. Radial and tangential forces

Another approach to the development of cyclorotor-based WECs was demonstrated in the PhD thesis of Nik Scharmann (Scharmann, 2018) in 2014. He proposed a 'Wave Hydro-mechanical Rotary Energy Converter' (WH-WEC) which should have 4 foils in order to minimise control requirements and stabilise the induced torque on the rotor shaft. The proposed design is based on the findings of experimental tests conducted in the Hamburg Ship Model Basin, Germany, as well as numerical simulation in Ansys Fluid and OpenFOAM. The CFD models were validated against each other, and the experimental results, in terms of the generated tangential F_T and radial F_R forces on the rotor foils.

The tangential F_T and radial F_R forces result from the lift F_L and drag F_D forces generated by a foil rotating in a fluid flow (see Fig. 3). Fundamentally, the lift and drag forces can be evaluated using the following equations:

$$F_L = \frac{1}{2}\rho\, C\, S\, C_L(\alpha)\, |\hat{V}|^2 \tag{11}$$

$$F_D = \frac{1}{2}\rho\, C\, S\, C_D(\alpha)\, |\hat{V}|^2, \tag{12}$$

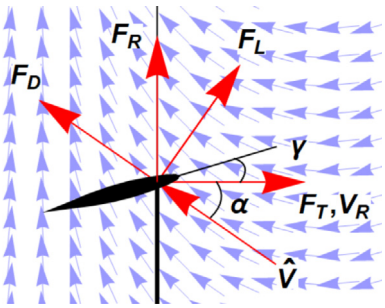

Fig. 3. Interaction between hydrofoil and wave induced fluid velocity.

where C and S are the length and span of the foil, respectively, $\hat{V}$ is the relative foil/fluid velocity, C_L and C_D are lift and drag coefficients, respectively, which are functions of the angle of attack α.

Then, the radial F_R and tangential F_T forces can be found as projections of the lift F_L and drag F_D forces on the tangent to the circular foil motion trajectory at the foil position, and at the normal to it, as:

$$F_T = F_L \sin(\alpha - \gamma) - F_D \cos(\alpha - \gamma) \tag{13}$$

$$F_R = F_L \cos(\alpha - \gamma) + F_D \sin(\alpha - \gamma). \tag{14}$$

where γ is a hydrofoil pitch angle.

Validation of the models in terms of tangential F_T and radial F_R forces has also been a focus of the LiftWEC project (Olbert et al., 2021; Ermakov et al., 2021; Ermakov and Ringwood, 2022). The benefit of this metric is that it allows the evaluation of lift C_L and drag C_D coefficients, which are important for estimation of the power which can be generated by the full-scale device. However, the model used did not consider losses due to the influence of the near wake foil hydrodynamics, free surface effects, and unsteady of foil hydrodynamics in waves (Gabriel and Ignazio, 2020). For example, the validation of such an approach against Scharmann's experiments (Scharmann, 2018), presented in Arredondo-Galeana et al. (2021), shows only moderate agreement with experimental results.

Nevertheless, this method had more successful application for the derivation of lift and drag coefficient in LiftWEC project experiments (Olbert et al., 2021; Ermakov and Ringwood, 2022). The 2D small-scale cyclorotor prototype, with one and two hydrofoils, was built and tested in a wave flume by Ecole Centrale de Nantes (ECN) (Thiebaut et al., 2021; Thiebaut and Payne, 2021a). Preliminary analysis of the results conducted in Olbert et al. (2021) show that evaluated lift and drag coefficients are close to the lift and drag coefficients which were obtained for airfoils in Sheldahl and Klimas (1981). However, attempts to use the derived coefficients in the Orcaflex model did not show good agreement with all of the experimental results (Olbert et al., 2021).

The most recent validation, in terms of radial and tangential forces for a cyclorotor with one hydrofoil, was conducted in Arredondo-Galeana et al. (2023b). The authors compare the generation of forces for the analysis of the point vortex (Ermakov and Ringwood, 2021a,b, 2022) and CFD models, and obtained good agreement for the case when the stall angle was not exceeded.

2.3. Mechanical power generation

An appealing (in terms of useful power) alternative to the assessment of cyclorotor performance in terms of wave cancellation (9) is the evaluation of the mechanical power generated on the rotor shaft (Ermakov et al., 2022a,b; Ringwood and Ermakov, 2022). Such a metric is well accepted for wind and tidal turbines. Mechanical power can be obtained as the product of rotational rate $\dot{\theta}(t)$ and power take off (PTO) torque $\mathcal{T}_{\mathcal{PTO}}$. Then, the average absorbed power, on a time interval $[0, T]$, can be calculated as:

$$P_{Shaft} = \frac{1}{T}\int_0^T \mathcal{T}_{PTO}(t)\dot{\theta}(t)dt \tag{15}$$

The PTO torque can be found from Newtown's second law for rotation as:

$$\mathcal{T}_{PTO} = \mathcal{T}_{Wave} - I\ddot{\theta}, \tag{16}$$

where I is the rotor inertia, $\ddot{\theta}$ the angular acceleration, and the wave induced torque $\mathcal{T}_{Wave}$ can be evaluated as:

$$\mathcal{T}_{Wave} = (F_{T_1} + F_{T_2})R, \tag{17}$$

The power integral in (15) also can be used for estimation of the power loss P_{Drag} due to the drag in Eq. (10) as proposed in (Siegel, 2019):

$$P_{Drag} = \frac{1}{T}\int_0^T F_D(t)R\dot{\theta}(t)dt \tag{18}$$

mechanical power evaluation can be considered as a more accurate metric (than wave cancellation) since it is more connected with the rotor generator. Such metrics have been used to assess the increase in generated power due to the control strategies developed in Ermakov et al. (2022a) and Ringwood and Ermakov (2022). The results presented in Ermakov et al. (2022b) show significant disagreement between shaft power P_{Shaft} and wave cancellation $P_{Cancelled}$ metrics, after implementation of an optimal variable rotational rate in monochromatic waves.

3. Determination of a mathematical point vortex model and its parameters

The point vortex model, introduced in Ermakov and Ringwood (2021a,b) and Ermakov and Ringwood (2021), proposed a near wake hydrodynamic hydrofoil model and derived a simplified potential for it. The cyclorotor model includes the assumptions of the previous researchers (Hermans et al., 1990; Fagley et al., 2012) and has been validated against their experimental and numerical results, in terms of free surface perturbation caused by hydrofoil rotation. Articles (Ermakov and Ringwood, 2021a,b) also compare the results of hydrofoil representation as a point vortex with representation as a 2D thin chord profile. It was proposed to consider lift C_L and drag C_D coefficients as tuning parameters, in order to achieve agreement between the two models.

The innovation of the point source model is based on the assumption that the lift F_L and drag F_D forces (Eqs. (11), (12)) are caused by the interaction of the rotation of hydrofoil i with an overall relative velocity $\hat{\mathbf{V}}_\mathbf{i}$, representing the vector difference between the wave induced fluid velocity $\mathbf{V}_{\mathbf{W}_\mathbf{i}}$ and the cyclorotor rotational velocity $\mathbf{V}_{\mathbf{R}_\mathbf{i}}$, plus the instantaneous radiation and influence of wakes left by the moving foils $\mathbf{V}_\mathbf{H}$:

$$\hat{\mathbf{V}}_\mathbf{i} = \mathbf{V}_{\mathbf{W}_\mathbf{i}} - \mathbf{V}_{\mathbf{R}_\mathbf{i}} + \mathbf{V}_{\mathbf{H}_\mathbf{i}} \tag{19}$$

This approach allows simulation of non-stationary effects caused by the wake trailing the hydrofoil. The velocity of the waves, radiated by the moving hydrofoil, can be found as:

$$\mathbf{V_H} = \frac{\partial \mathcal{F}(\mathbf{z}, \mathbf{t})}{\partial \mathbf{z}} = (\mathbf{V_H})_\mathbf{x} - \mathtt{i}\,(\mathbf{V_H})_\mathbf{y} \tag{20}$$

The authors in Ermakov and Ringwood (2021a,b) have found the analytical solution of the integral (1) by wave number k in the following form:

$$\mathcal{F}(z,t) = \frac{\Gamma(t)}{2\pi\,\mathtt{i}} Log\left[\frac{z-c(t)}{z-\tilde{c}(t)}\right] - \frac{2\mathtt{i}\sqrt{g}}{\pi}\int_0^t \frac{\Gamma(\tau)}{\sqrt{\mathtt{i}(z-\tilde{c}(\tau))}} D\left[\frac{\sqrt{g}(t-\tau)}{2\sqrt{\mathtt{i}(z-\tilde{c}(\tau))}}\right] d\tau \tag{21}$$

where $z = x + \mathtt{i}y$ is the coordinate on the complex plain, $c(\tau) = x(\tau) + \mathtt{i}y(\tau)$ is the previous position of the foil at dynamic time τ and $D(x)$ is the Dawson function (Dawson, 1897):

$$D(x) = e^{-x^2}\int_0^x e^{y^2} dy. \tag{22}$$

Then, the close fluid velocity field $\mathbf{V}_{\mathbf{H}_i}$ caused by the foil rotation can be presented as the sum of the wakes left by the moving foils $\mathbf{V}_{\mathbf{HW}_{\mathbf{i,j}}}$, and the instantaneous radiation from the other foil $\mathbf{V}_{\mathbf{HM}_\mathbf{j}}$, as:

$$\mathbf{V}_{\mathbf{H}_i} = \mathbf{V}_{\mathbf{HM}_\mathbf{j}} + \mathbf{V}_{\mathbf{HW}_\mathbf{i}} + \mathbf{V}_{\mathbf{HW}_\mathbf{j}} \tag{23}$$

The inclusion of the close fluid velocity field permits correction of the estimate of the angle of attack for the rotor foil:

$$\alpha_i(t) = \arcsin\left(\frac{(V_{R_i})_x * (\hat{V}_i)_y - (V_{R_i})_y * (\hat{V}_i)_x}{|V_{R_i}||\hat{V}_i|}\right) + \gamma_i \tag{24}$$

The proposed near wake hydrodynamic model has been successfully validated against CFD simulation in Arredondo-Galeana et al. (2023b). A comparison of the results shows that the hydrodynamic model estimates the mean loading on the foil within 15%, for attached flow conditions, but may underestimate loads for large values of angle of attack, due to vorticity and flow separation effects. However, such physical processes cause a harmful effect on structural loading and power generation, and should be avoided.

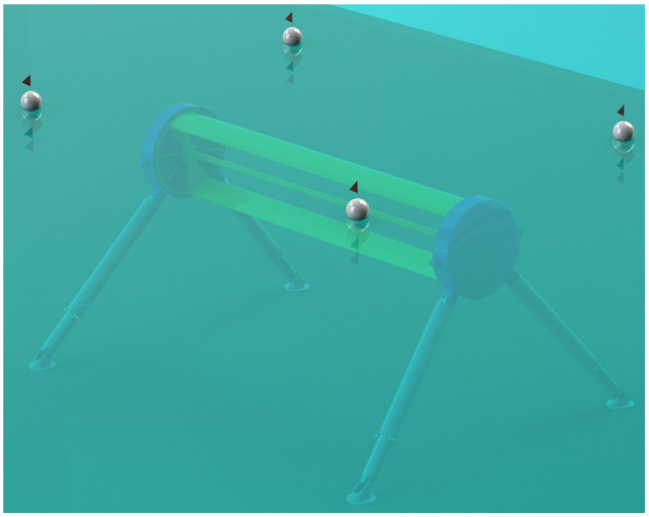

Fig. 4. The concept of CycWEC proposed in Siegel (2019).

In this article, we validate the point vortex model for the case of monochromatic waves. The velocity components $\mathbf{V_W}$ of the wave-induced water particle velocity can be found as the gradient of the Airy potential Eq. (5) as:

$$\mathbf{V_W} = \nabla \Phi_{\mathbf{W}} \tag{25}$$

The position (x_i, y_i) of hydrofoil i, and its instantaneous rotational velocity $\mathbf{V_R}$, can be found as:

$$x_i(t) = R\sin(\theta(t) + \pi(i-1)) \tag{26}$$

$$y_i(t) = y_0 + R\cos(\theta(t) + \pi(i-1)) \tag{27}$$

and

$$V_{Rx_i}(t) = R\dot{\theta}(t)\cos(\theta(t) + \pi(i-1)) \tag{28}$$

$$V_{Ry_i}(t) = -R\dot{\theta}(t)\sin(\theta(t) + \pi(i-1)) \tag{29}$$

respectively, where R is the radius of the rotor, y_0 is the submergence depth of the rotor centre, $\theta(t)$ is the polar coordinate of the hydrofoil, and $\dot{\theta}(t)$ is the rotor angular velocity.

4. Validation against the CycWEC workbench model in terms of power generation

In this section, we validate the point vortex model, in terms of shaft power P_{Shaft} and wave cancellation metrics P_{Cancel}, against the most recent performance assessment of the CycWEC presented in Siegel (2019). The CycWEC concept is illustrated in Fig. 4. The studied rotor has 2 hydrofoils with chord length $C = 5$ m, operational radius $R = 6$ m, and submergence depth $y_0 = -12$ m. We use identical lift and drag coefficients to Siegel (2019), from the same reference book (Sheldahl and Klimas, 1981), for symmetric hydrofoils NACA0015.

The performance assessment in Siegel (2019) was conducted using an average panchromatic wave power metric, based on the assumption of the ability of the rotor foils to maintain a consistently optimal stall attack angle, which would appear to be a challenging problem in the case of the stochastic motion of panchromatic wave particles. The metric in Siegel (2019) also considered 3D wave radiation effects, generator losses, and energy expended on control actions, while mixing the mechanical power of viscous losses, due to the drag force, and average wave cancellation power.

The control strategy in Siegel (2019) is based on the identification of the fundamental wave frequency in the spectrum of incoming panchromatic waves, which should be targeted for cancellation, by generating a wave with equal amplitude but opposite phase, using the cyclorotor. It is assumed that only the fundamental, corresponding to the monochromatic wave generated by the rotor, can extract energy from the incoming wave package, and this wave must have the following characteristics $\hat{T} = T_p$ and $\hat{H} = H_s/\sqrt{2}$, where T_p is the peak period and H_s the significant wave height.

In this study, we consider a two-dimensional model and assume that the generated power is linearly proportional to the shaft span of the rotor, assessed in [kW/m]. We model monochromatic incoming waves (5), with corresponding height $\hat{H}$ and period $\hat{T}$, and try to reproduce the power matrix (Fig. 5) from Siegel (2019). It is a challenging problem since, in our model, we consider a more exact pitch-wave particle interaction. However, this problem statement, for periodic monochromatic waves, allows us to obtain a constant and stable generated power assessment, and to study the influence

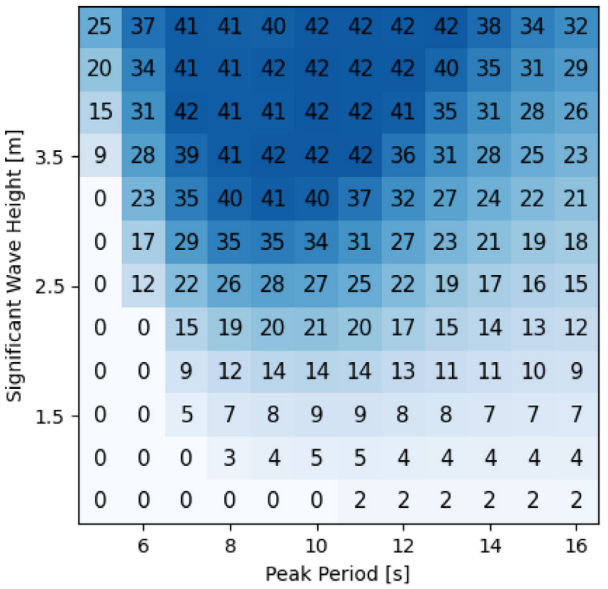

Fig. 5. Average shaft power evaluated for the CycWEC in Siegel (2019) and converted to kW/m.

of each velocity component. We assume that the cyclorotor rotates with the wave frequency, and the first hydrofoil has $\phi = 90^\circ$ relative phase with the crest of incoming waves (Ermakov et al., 2022a). We also calculate the free surface elevation caused by waves passing upstream and downstream at positions corresponding to one wave length $\pm\lambda$ from the cyclorotor position during the period T, after stable periodic wave cancellation and radiation is achieved (Ermakov et al., 2022b).

Our first estimate of cyclorotor performance, in terms of P_{Shaft} and $P_{Cancelled}$, for neutral values of pitch angles $\gamma_i(t) = 0$, provided us with significantly lower values, in comparison with the results of (Fig. 5). This is due to the consideration of a variable, and consistently optimal, attack angle in Siegel (2019), which ensures maximum circulation and, as a result, significantly increases the amplitude of the inverse-phase generated wave, and results in significantly greater lift forces.

For the next step, we carried out numerical optimisation (using a brute force algorithm) in search of the optimal *constant* pitch angles γ_i for each of the presented sea states, which allows us to minimise deviations from the reference values of Fig. 5. Fig. 6(a,b) presents tables of the obtained optimised constant pitch values for γ_2, (where $\gamma_2 = -\gamma_1$), while Fig. 6(c,d) shows the relative difference between the results obtained in Siegel (2019) and our estimates of mechanical power, or wave cancellation power generation, for the corresponding constant pitch angles.

In Siegel (2019), a variable *optimal* pitch angle was assumed at all times, and adjusted instantly by a mechanical actuator. However, we have shown in this study that we can obtain similar results, for most sea states, with a constant pitch angle, for the presented model, in terms of the $P_{Cancelled}$ metric. For larger values of T_p and H_s, we cannot reach the performance values of Fig. 5 using constant optimal pitch; such values can only be achieved by implementation of a perfect real-time control strategy, as presumed in Siegel (2019).

Further investigation of the difference between mechanical and the wave cancellation metrics has shown that $P_{Cancelled}$ is approximately 30% more optimistic than the mechanical power generation metric P_{Shaft} (this issue is also articulated in Ermakov et al. (2022b) for the real-time control case). Fig. 7 highlights the relative difference between the shaft power and wave cancellation metrics, for neutral pitch values $\gamma_i = 0$, for various types of monochromatic waves. Fig. 7 also highlights significant differences for waves with short period and small wave height. These differences can be explained by the fact that, in the wave cancellation metric, the energy of the incoming wave is partly absorbed by the cyclorotor, through the generation of a similar but anti-phase wave, caused by circulation. Circulation is therefore responsible for the absorbed power, the remainder of the incoming energy being transmitted downstream or reflected upstream. Circulation also provides information about the lift forces acting on the hydrofoils, via Eq. (2). However, only the tangential part of the lift force is responsible for energy generation, while the balance of the absorbed power, conveyed by the normal component of the lift force, cannot act usefully on the cyclorotor. This energy loss is not taken into account in the wave cancellation metric and can explain its relative optimism. Accordingly, the advantage of the mechanical power generation metric is that its estimate is based on PTO torque, directly linked to the tangential components of the lift and drag forces (see Eqs. (11) and (12)) and has a strong link to electrical power generation.

In general, the mechanical power estimates (Fig. 6(c)) are 30% lower than the results obtained by the Atargis energy corporation (Fig. 5). However, the assessment is conducted for a constant rotational velocity and constant optimal pitch values. The implementation of real time control for velocity and pitch can increase the generated power by 30%–40%

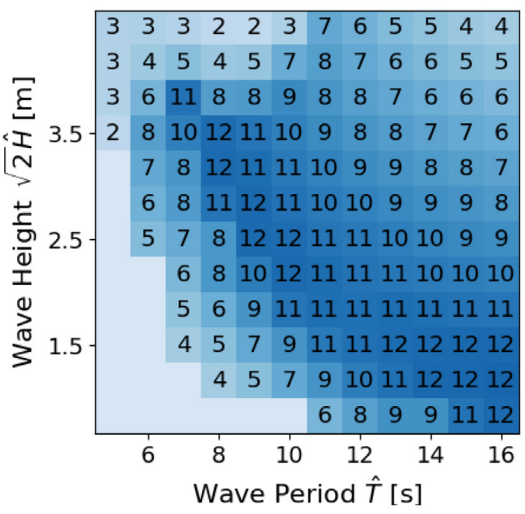

(a) Optimal pitch γ_2 values for P_{Shaft} metric

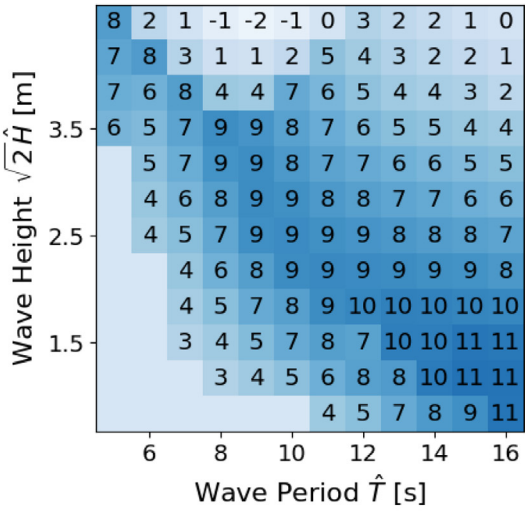

(b) Optimal pitch γ_2 values for $P_{Cancelled}$ metric

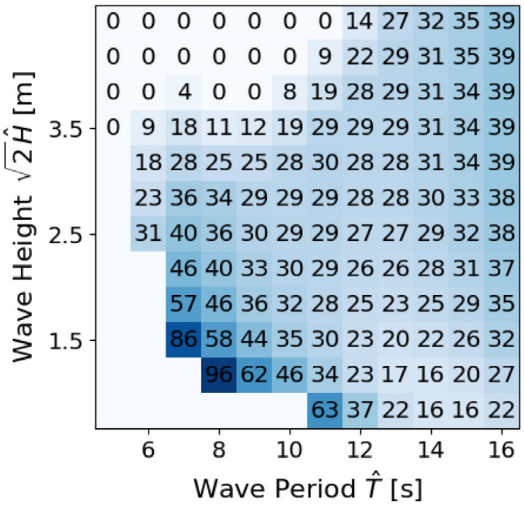

(c) Difference between power assessed in (Siegel, 2019) and P_{Shaft} in %

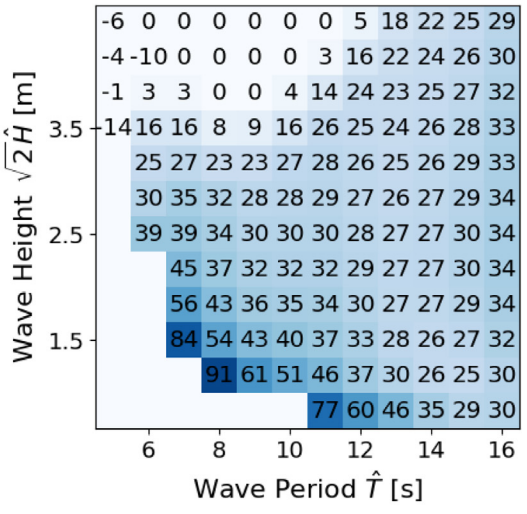

(d) Difference between power assessed in (Siegel, 2019) and $P_{Cancelled}$ in %

Fig. 6. Optimal constant pitch angle values for the P_{Shaft} and $P_{Cancelled}$ metrics (a,b), and the corresponding relative difference between the results obtained in Siegel (2019) and our estimates of mechanical power (c) and wave cancellation power (d).

as shown in Ermakov et al. (2022a) and Ringwood and Ermakov (2022). Thus, the power assessment conducted by Atargis (Siegel, 2019) can be considered as confirmed, since the CycWEC concept assumes real-time control of pitch and rotational velocity.

5. Validation against the results of experimental testing of the 2D LiftWEC prototype

5.1. Experimental setup, assumptions, and levels of accuracy

This section is dedicated to the validation of the point vortex model against the recent 2D experimental tests of the LiftWEC cyclorotor (see Fig. 8(a)). The 2D LiftWEC prototype was designed, built and tested by Ecole Centrale Nantes (ECN), France. The experimental data, and test description documentation, are published in open access on Zenodo (Thiebaut et al., 2021; Thiebaut and Payne, 2021a). The validations presented in this article use the same experiment numbering system as the experimental data sets.

The 2D LiftWEC prototype allows the installation of one or two curved foils NACA0015, with chord lengths $C = 0.3$ m, and span $S = 0.49$ m. The cyclorotor has a radius $R = 0.3$ m and a submergence depth of the rotor axis at $y_0 = -0.755$ m.

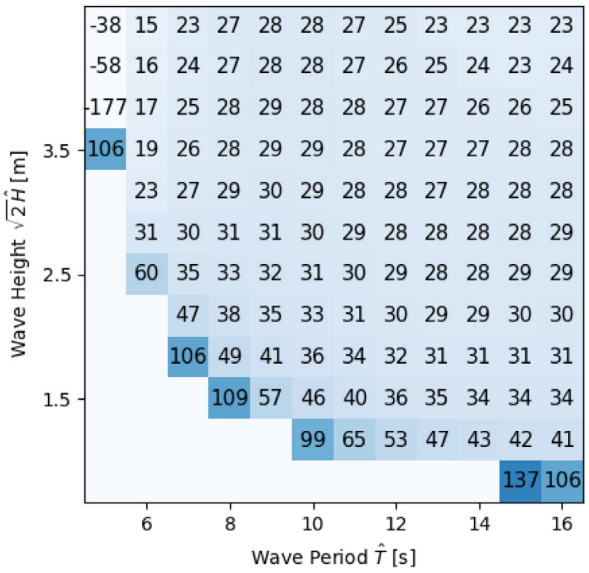

Fig. 7. Relative difference between wave power changes P_{Cancel} and mechanical power generation P_{Shaft} for neutral pitch angle.

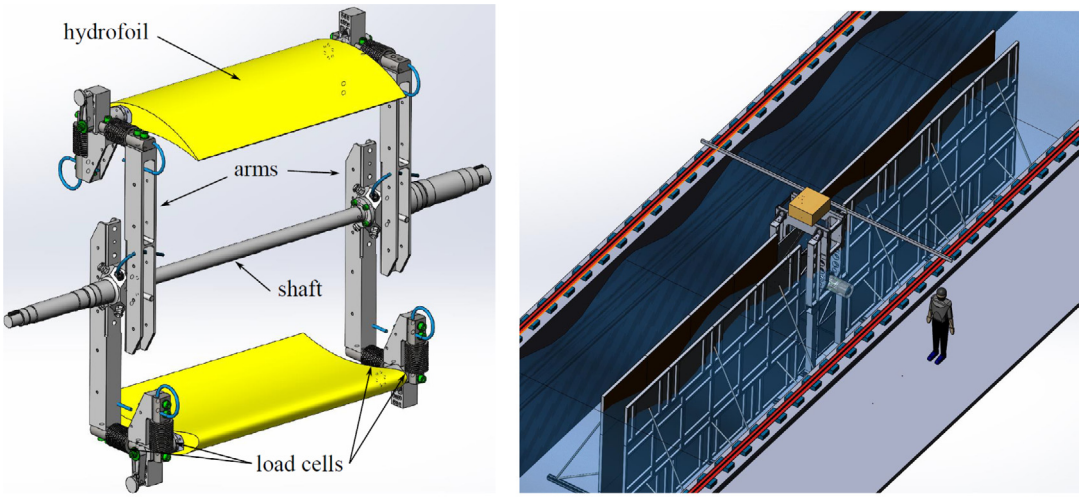

(a) Experimental prototype of the 2D LiftWEC. (b) Experimental setup of the 2D LiftWEC.

Fig. 8. Experimental prototype and setup of the 2D LiftWEC.

The experimenters adjusted hydrofoil pitch angles manually between tests. The rotational speed of the 2D LiftWEC is controlled using a PTO defined system which consists of an electrical motor which can be controlled in both speed and torque. The installed sensors permit measurement of the PTO torque, radial and tangential loading, and the position of the hydrofoils in polar coordinates (see Fig. 8(a)). The measured position data allows estimation of rotational velocity and acceleration; however, the raw position measurement is subject to noise and this error propagates in the estimation of velocity and acceleration.

The LiftWEC prototype has been tested in the ECN wave and towing tank, in a narrow 'sub-channel' confined with partition walls, which reduce the flume width locally (Fig. 8(b)). Fairings were designed to mask the arms of the rotor and to ensure that the foils are subject to 2D flow conditions. They were designed as discs, which are visible in Fig. 9, showing the experimental setup. A set of wave gauges was installed inside the sub-channel to measure surface elevation and for wave calibration. Such an experimental setup allows the use of a tank capable of generating large waves while keeping the narrow width of the device. Unfortunately, it led to the generation of parasitic waves at the inlet and outlet of the sub-channel (Fig. 8(b)). While the influence of the waves reflected from the inlet can be ignored, the waves reflected from the outlet cause a significant disturbance to the experimental data. Such a problem had not been expected during

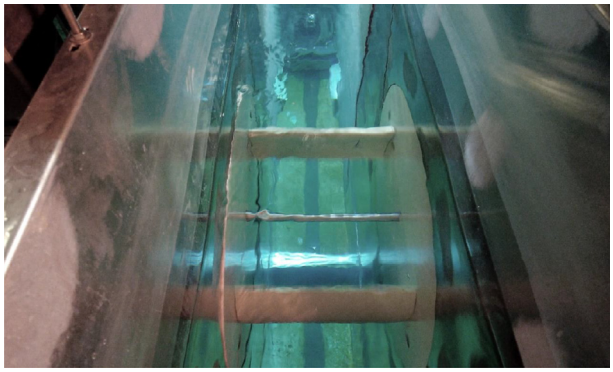

Fig. 9. Rotor with fairings in a sub-canal during experiments.

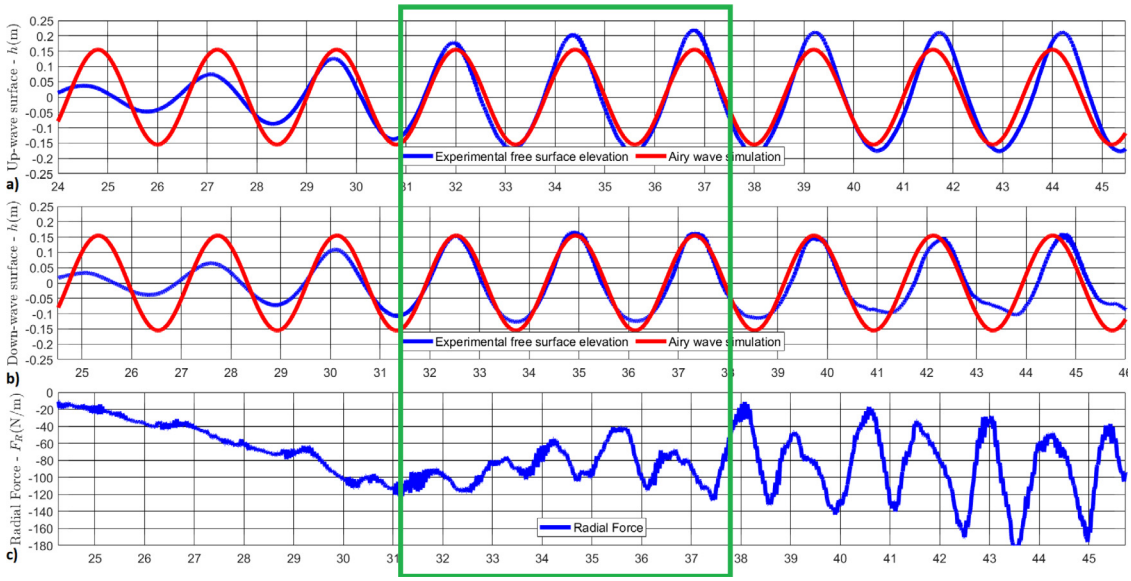

Fig. 10. Determination of the time-frame for experimental data analysis, Test 114. In Test 114 a single hydrofoil with pitch $\gamma = 0°$ rotates in regular wave $H = 0.31$ m, $T = 2.4$ s with the phase $\phi = 90°$. (For interpretation of the references to colour in this figure legend, the reader is referred to the web version of this article.)

the planning of experiments. The effect is explained by the discontinuity between the wave field inside and outside of the sub-channel. The assessment of the reflection conducted during the wave calibration runs is based on the standard Mansard and Funke approach (Olbert et al., 2021). The obtained values of the reflection coefficients are evaluated as 22% on average, for the various generated waves. In our validation, we mitigate such effects by using the parts of the time series data obtained before the waves reflected from outlet reaches the cyclorotor.

Fig. 10 illustrates the selection of the time frame for analysis, based on the free surface elevation up-wave, down-wave, and corresponding changes in the radial force for Test number 114. In this experiment, a single hydrofoil with pitch $\gamma = 0°$ rotates in a regular wave $H = 0.31$ m, $T = 2.4$ s, with phase $\phi = 90°$. The free surface elevation data from 'Gauge 4', located 1 m up-wave from the cyclorotor, and 'Gauge 6', located 1 m down-wave from the cyclorotor, are used for modelling the incident and transmitted waves. The blue lines correspond to the experimental data while the red line is the analytical Airy wave (6) approximation of the free surface perturbation caused by the incident (a) and transmitted (b) waves. The time interval from 25 to 31 s in Fig. 10 shows the development of the incoming wave, and cannot be used for analysis, while the intervals from 38 to 46 s in Fig. 10(b) shows the influence of the reflected waves, which cause significant fluctuation of the radial force (Fig. 10(c)). As a result, only the short time window from 31 to 38 s can be used for data analysis. The selected time interval shows the reasonable fluctuation of the radial force, in Fig. 10(c), and wave cancellation effects, in Fig. 10(a,b).

Unfortunately, due to the short time frame, and significant radiation from the sub-canal inlet and outlet, it is not possible to apply the wave cancellation metrics for device performance assessment. As has been shown before (Fig. 2),

it requires at least 8 full rotational periods in monochromatic waves to stabilise wave cancellation, while most of the experimental time frames are limited to just 3 full rotations (see Fig. 10).

Another problem which was encountered during the experiments is the transfer of the positive effect of the generated lift force to the rotor shaft. While the force load cells (located directly on each side of the foils) show generation of the positive tangential force on the foils, the shaft-based torque meter shows negative power generation. Such a contradiction is explained by the power losses due to the additional torque generated by the drag force on the arms connecting the hydrofoils to the rotor shaft (Olbert, 2022). Such a problem requires an engineering solution for optimal cyclorotor design or, for example, installation of the PTO directly on the hydrofoils. Nevertheless, stable power generation, in terms of the shaft power, for the LiftWEC project was obtained only later during the 3D testing campaign (Thiebaut and Payne, 2021b). Therefore, we can only validate the developed point source model against the 2D test data in terms of the forces generated on the hydrofoils.

5.2. Analysis of lift and drag forces for rotating hydrofoils

All of the published performance assessment for cyclorotor-based WECs was conducted with the use of the lift and drag coefficients which were obtained for straight airfoils in ideal conditions of aerodynamic tubes (Siegel, 2014, 2019; Ermakov and Ringwood, 2021c). Now, we question the equivalence between aerofoils and hydrofoils in waves, in terms lift and drag coefficients.

The published analytical assessment of device performance has shown that a cyclorotor achieves maximum performance, in terms of wave cancellation (Siegel, 2019), or mechanical shaft power generation (Ermakov et al., 2022a), when its hydrofoils operate in the vicinity of the stall angle of attack. Similar results were confirmed during constant pitch optimisation conducted in Section 3. However, as has been shown in Arredondo-Galeana et al. (2023b), the operation at such a high angle of attack may lead to flow separation.

This subsection is dedicated to the methodology related to the derivation and assessment of the lift C_L and drag C_D coefficients, from the 2D experimental results, using the *nonlinear* point vortex model which considers non-stationary effects caused by the wakes. Preliminary *linear* estimates of the lift and drag coefficients were determined in LiftWEC project deliverable (Olbert et al., 2021) using pseudo-stationary model. However, application of the derived coefficients, in the Orcaflex model, did not show acceptable results (Olbert et al., 2021).

In this article, the authors consider *nonlinear* effects of the instantaneous radiation and wakes left by the rotating foils. The lift and drag coefficients are also considered not only as functions of the angles of attack and Reynolds number, but also as functions of the foil submergence and velocity, in order to account for complex hydrodynamic effects (such as stall delay, load hysteresis and dynamic stall Gabriel and Ignazio, 2020), which cannot be included in the simplified control oriented model (Ermakov and Ringwood, 2021a).

The values of the C_L and C_D are estimated from experimentally measured values of tangential $F_{T_{cell_i}}$ and radial $F_{R_{cell_i}}$ forces. The data is recorded from load cells installed between the hydrofoils and the cyclorotor arms (Fig. 8(a)). The measured loading can be converted to a two-dimensional model by summation of two measurements from the opposite corresponding coupled sensors, and subsequent division by the foil span S:

$$F_{T_{2D}} = (F_{T_{cell_1}} + F_{T_{cell_2}})/S \tag{30}$$

$$F_{R_{2D}} = (F_{R_{cell_1}} + F_{R_{cell_2}})/S \tag{31}$$

The direction of forces and the half-chord position, provided from the tank test, does not match the quarter-chord oriented coordinate system of the point vortex (Fig. 11). Therefore, we apply a 14.5° shift correction, and consider the location of the point vortex on the quarter chord (Olbert et al., 2021):

$$\tilde{F}_T = F_{T_{2D}} \cos(14.5^\circ) - F_{R_{2D}} \sin(14.5^\circ) \tag{32}$$

$$\tilde{F}_R = F_{T_{2D}} \sin(14.5^\circ) + F_{R_{2D}} \cos(14.5^\circ) \tag{33}$$

$$\theta_{2D} = \theta + 14.5^\circ \tag{34}$$

The shifted and corrected values of the tangential F_T and radial F_R force are used in the analytical point vortex model for estimation of the lift C_L and drag C_D coefficients using systems (13) and (14).

5.3. Model validation for rotation of a hydrofoil in still water

Fig. 12(a,b) illustrates the estimated values of the lift C_L and drag C_D coefficients from Test 165. In Test 165, a single hydrofoil with an adjusted pitch angle $\gamma = -4^\circ$ is rotated in still water, with frequency $\dot{\theta} = 2$ rad/s. Due to the absence of incoming waves, the wave-induced fluid velocity $\mathbf{V_W}$ in Eq. (19) is zero. However, the difference in distance between the point vortex and its mirror, throughout the rotation, as well as the influence of the generated wake, will lead to different induced velocities $\mathbf{V_{HW}}$ and thus different angles of attack, with $\alpha = -3.1^\circ$ at the upper $\theta = 40^\circ$ and $\alpha = -4.5^\circ$ at the lower $\theta = 280^\circ$ positions.

As can be seen from Fig. 12(a,b), the values of the lift and drag coefficients are more sensitive to the position of the hydrofoil than to the angle of attack. The increase in the lift coefficient, despite a decrease in the angle of attack, when

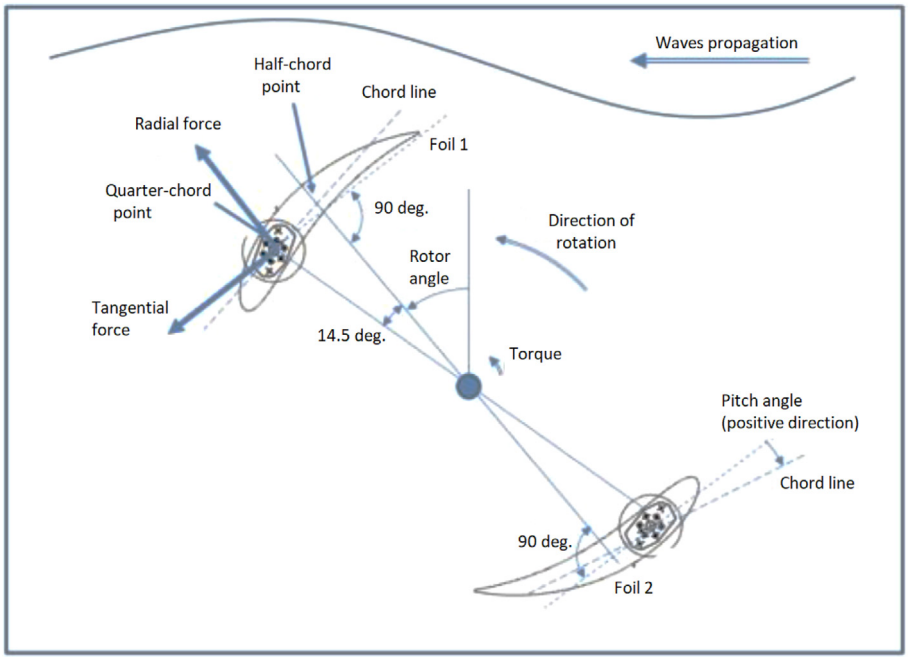

Fig. 11. Schematic draft of the experimental setup.

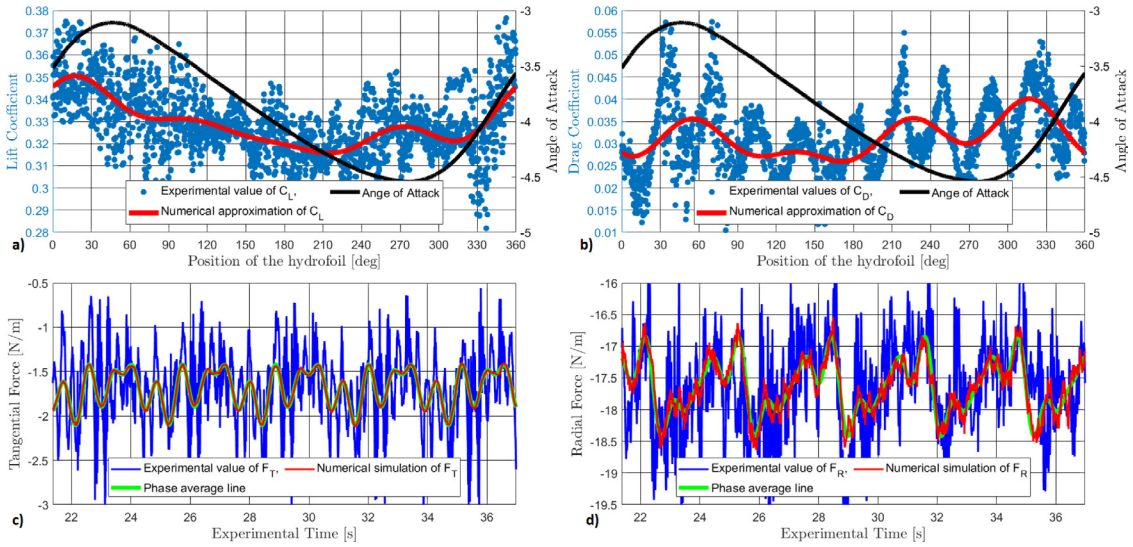

Fig. 12. Derivation of the lift and drag coefficients (a,b) and their validation against the experimental data (c,d) for Test 165. In Test 165 a single hydrofoil with the adjusted pitch angle $\gamma = -4°$ rotated in still water with the frequency $\dot{\theta} = 2$ rad/s. (For interpretation of the references to colour in this figure legend, the reader is referred to the web version of this article.)

the hydrofoil approaches the free surface $\theta = 0°$ or $360°$, can be explained by the increase in circulation. As was also shown in Gabriel and Ignazio (2020), Lei et al. (2022b) and Lei et al. (2022a), rotor blades can experience unsteady effects such as stall delay, load hysteresis, and dynamic stall. The drag coefficients also behave differently for each quadrant of the circular trajectory. Thus, it is important to consider lift and drag coefficients, not only as functions of the angle of attack and Reynolds number, but also as functions of the position of the foil and direction of its movement. Of course, such coefficients can be determined only from experimental test data, or hi-fidelity CFD simulation. A similar approach is used for estimation of wave diffraction coefficients for traditional point absorber WECs (Penalba et al., 2017).

The considered lift and drag coefficients are therefore approximated using the trend represented by a Fourier series with 4 harmonics, in order to separate the signal from the noise (see Fig. 13(c,d)). The appropriate Reynolds number for

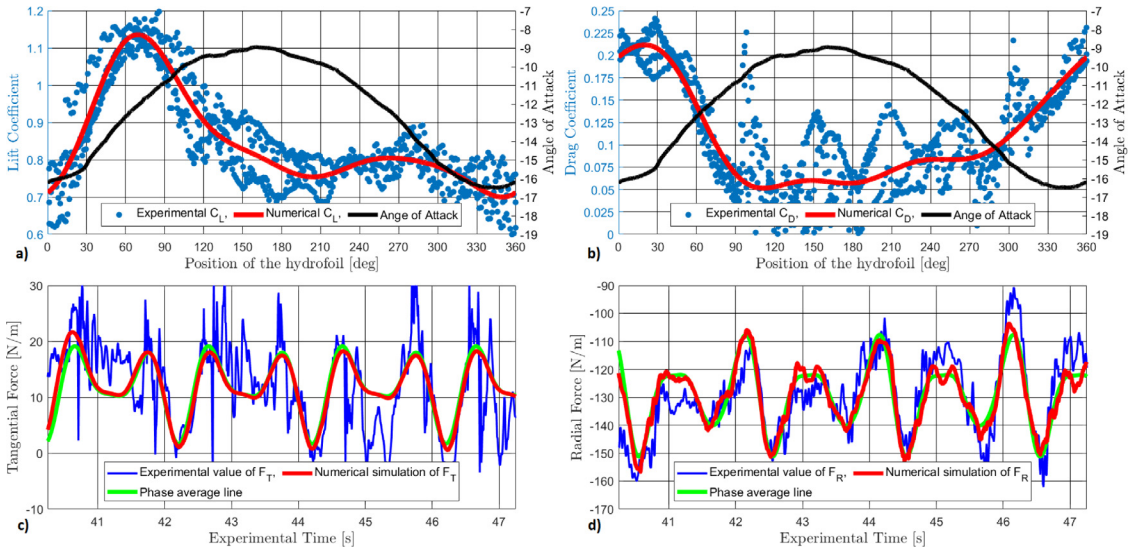

Fig. 13. Derivation of the lift and drag coefficients (a,b) and their validation against experimental data (c,d) for Test 112. In Test 112, a hydrofoil with zero pitch angle $\gamma = 0$ was rotated in monochromatic wave $H = 0.31$ m and $T = 2$ s, with the wave frequency $\dot{\theta} = \omega$ and relative phase $\phi = 90°$. (For interpretation of the references to colour in this figure legend, the reader is referred to the web version of this article.)

the adopted conditions is $Re \approx 137\,500$. The obtained lift coefficient for $\alpha = -4°$ is smaller than the corresponding lift coefficient for a airfoil NACA0015 (Sheldahl and Klimas, 1981), which is $C_L = 0.4186$ for $Re = 80\,000$, and $C_L = 0.44$ for $Re = 160\,000$. The curved hydrofoil also experiences much more significant drag than a straight airfoil, for which drag coefficient $C_D = 0.0168$ for $Re = 80\,000$, and $C_D = 0.0132$ for $Re = 160\,000$.

Fig. 12(c,d) illustrates the validation results for the derived lift and drag coefficients, showing good agreement with the experimental data for the tangential and radial forces.

5.4. Model validation for rotation of a hydrofoil in waves

In this subsection, we study the applicability of the developed approach for simulation of a hydrofoil rotating in waves. The incoming regular wave is approximated by an Airy wave, Eq. (6). The wave amplitude H, period T, and wave number k are defined by experimental parameters, while the phase ϕ is evaluated to satisfy the free surface elevation period at the up-wave and down-wave gauges, located one metre up-wave and down-wave of the cyclorotor (see Fig. 2). Fig. 10 illustrates good agreement between experimental measurements and the proposed mathematical model, for the set of test incident waves. The validated approximation of the incoming wave by an Airy wave potential (5) also allows determination of the wave induced fluid velocity field $\mathbf{V_W}$ in the vicinity of the hydrofoils, via Eq. (25).

Fig. 13(a,b) illustrates the lift and drag coefficients derived for Test number 112. Test 112 is selected because, for this case, the hydrofoil NACA0015 operates in the vicinity of the stall angle $\alpha_{stall} = 15°$ for which the maximum power is generated in simulations conducted in Siegel (2019) and in Section 4. In Test 112, a hydrofoil with the zero pitch angle $\gamma = 0$ is rotated in monochromatic waves with $H = 0.31$ m and $T = 2$ s, with the wave frequency $\dot{\theta} = \omega$, and relative phase $\phi = 90°$. The lift and drag coefficients are obtained for the time interval from 40.25 to 47.25 s, which is relatively clear of wave reflections.

The horizontal axis in Fig. 13(a,b) represents the position of the foil (in degrees) where 0° corresponds to the foil at top dead centre. The left vertical axis of Fig. 13(a,b) corresponds to the experimentally measured lift coefficient values (blue points), and their analytical trend (red line), while the right vertical axis corresponds to the estimated angles of attack for different foil positions (black line). It can be seen, from Fig. 13(a), that the lift coefficient achieves its extremum twice over the plotted period, when $\alpha = -12°$, with maximum lift occurring when the hydrofoil moves towards its lowest point in the cycle ($\theta = 70°, C_L = 1.15$), but with a weaker response when the foil approaches the free surface ($\theta = 250°, C_L = 0.8$). Such a difference can be explained by the unsteady hydrodynamics of hydrofoils, specifically flow separation and deep dynamic stall effects (Gabriel and Ignazio, 2020). Such effects can significantly decrease the realistic potential performance of a cyclorotor.

The lift and drag coefficients determined within the assumptions of the model depend not only on the angle of attack and Reynolds number, but also on the position of the foil and the direction of movement. It allows faithful reproduction of the experimental measurements. Fig. 13(c,d) illustrates good validation against experimentally measured tangential and radial forces, after implementation of the proposed approach. The lift and drag coefficients determined from the experimental data may include effects not included in the parametric structure of our model i.e. the calculated lift and

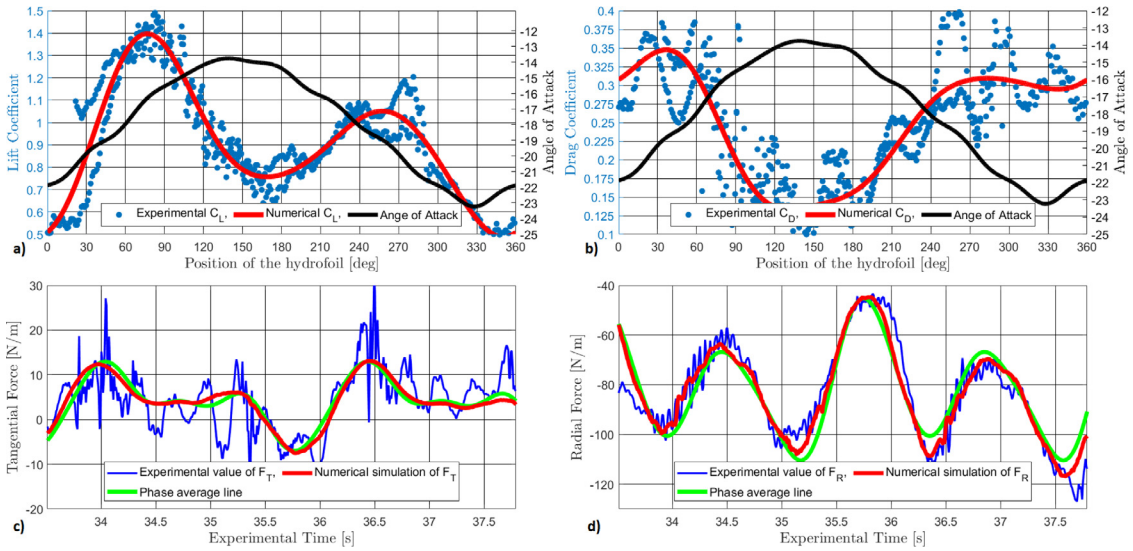

Fig. 14. Derivation of the lift (a) and drag (b) coefficients and their validation against the experimental data (c,d), for Test 114. In Test 114, a single hydrofoil with pitch $\gamma = 0°$ rotates in monochromatic waves with $H = 0.31$ m, $T = 2.4$ s, and relative phase $\phi = 90°$. (For interpretation of the references to colour in this figure legend, the reader is referred to the web version of this article.)

drag coefficients may contain effects due to unmodelled dynamics. In that sense, the lift and drag coefficients are 'tuned' to best fit the experimental data. However, given the relatively close agreement between the (experimentally) calculated coefficients, and those obtained from reference NACA0015 foil data, it appears that the parametric structure of the model is relatively sound, so the reliance on the data (and the specificity of the wave condition), in relation to other unmodelled dynamics, is relatively light. Nevertheless, accurate prediction of the lift and drag coefficients for foils in deep stall is a challenging problem, and stall can be avoided using the control method proposed by the Atargis Energy Corporation (2022). However, significant further research and technology development may allow such effects to be exploited, which could potentially increase the performance of cyclorotor devices.

A second example is dedicated to the study of lift and drag coefficient behaviour, for large values of attack angle, and to validation of Test 114, for which the time interval is defined in Section 5.1 in Fig. 10. In this experimental model, a single hydrofoil with pitch $\gamma = 0°$ rotates in regular waves with $H = 0.31$ m, $T = 2.4$ s, and relative phase $\phi = 90°$. The derived lift and drag coefficients are presented in Fig. 14(a,b), clearly showing that the hydrofoils experience a range of angles of attacks from $-14°$ to $-24°$. The lift coefficient achieves a second maximum at $\alpha = -16°$. This maximum also corresponds to the same hydrofoil position $\theta = 70°$ as in Test 112. It can be concluded that the foil experiences some parametric resonance at this position. The largest estimated value of the lift coefficient $C_L \approx 1.5$ for $\alpha = -16°$ even exceeds the maximum lift coefficient obtained in Wehausen and Laitone (1960) for an airfoil, which is $C_L = 1.4233$ for a much larger Reynolds number $Re = 10^7$. However, the hydrofoil also experiences significantly greater drag, of $C_D \approx 0.3$, while $C_D = 0.197$ is the maximum for an aerofoil, for a similar angle of attack.

5.5. Model validation for rotation of a twin-foil cyclorotor in waves

In this subsection, we analyse the influence of the installation of a second hydrofoil on the lift and drag coefficients of the first one. For this purpose, Test number 191 is selected, which has the same wave conditions as Test 114 (Section 5.4) for a single hydrofoil, for which the maximum lift coefficient is obtained.

In Test 191, two hydrofoils with neutral pitch $\gamma_{1,2} = 0$, rotate with the wave frequency $\dot{\theta} = \omega$ in monochromatic waves with $T = 2.4$ s, $H = 0.31$ m, and with relative phase $\phi = 90°$ for the first hydrofoil. Comparison of the results for the single foil (Fig. 14) and two foil (Fig. 15) cases shows a significant drop in lift and drag coefficients for the first foil of the two foil prototype. Such effects can be explained by the significant perturbation of the fluid field caused by the twin-foil rotor, resulting in a scattering of wave-induced water circulation, and a decrease in hydrodynamic load on the foil surfaces. Generally speaking, the foils are operating in turbulent wakes left by each other, resulting in non-homogeneous foil surface pressure and more significant differences in the angle of attack at each of the foil surface points. Nevertheless, the developed analytical model has enough flexibility to approximate such a complex hydrodynamics process, as can be seen from the successful validation in terms of the tangential and radial forces (see Fig. 15(c,d)).

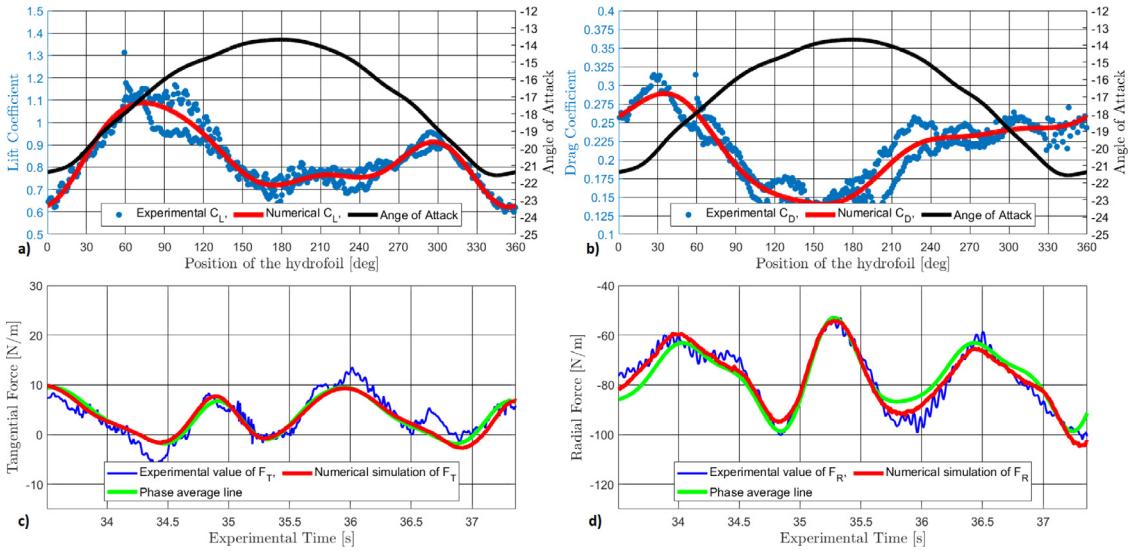

Fig. 15. Derivation of the lift and drag coefficients (a,b) for the first hydrofoil, under the influence of the wake from the second foil, and their validation against the experimental data (c,d) for Test 191. In Test 191, two hydrofoils with neutral pitch $\gamma_{1,2} = 0$ rotate with the wave frequency $\dot{\theta} = \omega$ in monochromatic waves with $T = 2.4$ s, $H = 0.31$ m, and relative phase $\phi = 90°$ for the first hydrofoil. (For interpretation of the references to colour in this figure legend, the reader is referred to the web version of this article.)

6. Conclusion

6.1. Applicability of the model

The conducted analysis has shown that a control-oriented point vortex model can describe the rotation of a cyclorotor WEC in water waves, generation of forces, and mechanical power, as well as wave cancellation. It allows us to reproduce the results of previously conducted numerical and experimental study of the cyclorotor WEC (Siegel, 2019; Ermakov and Ringwood, 2021a, 2022). The model puts into perspective previous cyclorotor WEC performance assessment (i.e. Atargis results may be slightly optimistic) and the use of wave cancellation may not be the best performance metric, given that converted power is the ultimate objective.

The point vortex model helps us to understand and explain some mechanical and hydrodynamic effects identified during the experimental ECN test campaign, also facilitating estimation of lift and drag coefficients from the experimental data, and simulation of the forces generated on the hydrofoils. In general, validation of the model against experimental results is successful and the authors recommend the point vortex model for further control design and performance assessment studies.

6.2. Limitations and simplifications

The presented validation of the point source model is limited to the 2D monochromatic wave case. Nevertheless, the obtained values of lift and drag coefficients are realistic and comparable with the lift and drag coefficients which were obtained for aerofoils (Sheldahl and Klimas, 1981). These coefficients can be used for development of optimal control strategies for more complex panchromatic sea states using methods which were developed in Ermakov et al. (2022a), Ringwood and Ermakov (2022) and Arredondo-Galeana et al. (2023a).

Application of the developed model for optimal control developed in Ermakov et al. (2022a) or performance assessment would require development of tables of approximate lift and drag coefficients, which need to be estimated from experimental tests or hi-fidelity CFD simulation. Such coefficients should be considered not only as function of the angle of attack and Reynolds number but also the position of the foil and the direction of its movement and have considerable computational implications. The determination of the optimal location of a relative point source on a hydrofoil chord, for estimation of angles of attack, requires additional investigation. The model does not consider complex nonlinear wave/foil hydrodynamic interaction effects, nor mechanical nonlinearity, such as additional torque induced by drag on the rotor arms. However, such simplifications allow us to significantly decrease the model computation time, making the model suitable for real-time control calculations. Application of the validated model for real-time control will require further development of estimators and predictors for directly unmeasurable key control variables, as well as actuators, electronics, and generator models.

6.3. Problems and perspectives

Analysis of experimental data has revealed a range of new challenges for cyclorotor WEC technology, which need to be solved by structural design optimisation. Twin hydrofoil concepts involve foil operation within the wake of the preceding foil, resulting in significant fluid perturbation which, along with the long hydrofoil chord, make it impossible to achieve the optimal angle of attack. The length of the chord probably should be reduced to avoid uncertainty in the actual angle of attack and difference in pressure along the foil surface. The transfer of generated lift forces to the rotor shaft could incur significant losses, due to drag forces on the structure connecting the hydrofoils to the rotor shaft. This could possibly be mitigated by optimising the shape of these connecting arms. The experimental Reynolds number of 137 500, for a NACA0015 foil, is in a range where, even under optimal conditions in very clean wind tunnels, it is difficult to maintain attached flow. Crucially, it may be better to develop specialised foils dedicated to rotation in wave conditions, rather than use foils which are optimised for relatively low Reynolds conditions. New foils could also potentially reduce drag losses.

Nevertheless, analysis of the experimental data confirms that the generation of lift force and estimated lift coefficients are comparable with values measured for airfoils. It creates motivation for further development of this technology.

CRediT authorship contribution statement

Andrei Ermakov: Writing – original draft, Conceptualization, Methodology, Validation, Investigation. **Florent Thiebaut:** Writing – review & editing, Conceptualization, Validation, Investigation. **Grégory S. Payne:** Writing – review & editing, Conceptualization, Validation, Investigation. **John V. Ringwood:** Writing – review & editing, Conceptualization, Supervision, Funding acquisition.

Declaration of competing interest

The authors declare that they have no known competing financial interests or personal relationships that could have appeared to influence the work reported in this paper.

Data availability

The authors used data which is published in open access. It is referenced in the article

References

Arguilé-Pérez, B., Ribeiro, A.S., Costoya, X., De-Castro, M., Carracedo, P., Dias, J.M., Rusu, L., Gómez-Gesteira, M., 2022. Harnessing of different WECs to harvest wave energy along the Galician coast (NW Spain). J. Mar. Sci. Eng. 10 (6).

Arredondo-Galeana, A., Ermakov, A., Shi, W., Ringwood, J.V., Brennan, F., 2023a. Control strategies for power enhancement and fatigue damage mitigation of wave cycloidal rotors.

Arredondo-Galeana, A., Olbert, G., Shi, W., Brennan, F., 2023b. Near wake hydrodynamics and structural design of a single foil cycloidal rotor in regular waves. https://ssrn.com/abstract=4239352 (accessed 03 February 2023).

Arredondo-Galeana, A., Shi, W., Olbert, G., Scharf, M., Ermakov, A., Ringwood, J.V., Brennan, F., 2021. A methodology for the structural design of LiftWEC: A wave-bladed cyclorotor. In: Proceedings of 14th European Wave and Tidal Energy Conference. Plymouth, UK, Paper #1967.

2022. Atargis energy corporation. https://atargis.com// (accessed 03 February 2023).

Batchelor, G.K., 1967. An Introduction to Fluid Dynamics. Cambridge University Press, p. 406.

Caskey, C.J., 2014. Analysis of a Cycloidal Wave Energy Converter using Unsteady Reynolds Averaged Navier-Stokes Simulation (Master's thesis). University of New Brunswick, USA.

Chitale, K.C., Fagley, C., Mohtat, A., Siegel, S.G., 2021. Numerical evaluation of climate scatter performance of a cycloidal wave energy converter. In: Proceedings of 14th European Wave and Tidal Energy Conference. Plymouth, UK, Paper #2141.

Dawson, H.G., 1897. On the numerical value of $\int_0^h e^{x^2}\,dx$. Proc. Lond. Math. Soc. s1-29 (1), 519–522.

Ermakov, A., Marie, A., Ringwood, J.V., 2022a. Optimal control of pitch and rotational velocity for a cyclorotor wave energy device. IEEE Trans. Sustain. Energy 13 (3), 1631–1640.

Ermakov, A., Marie, A., Ringwood, J.V., 2022b. Some fundamental results for cyclorotor wave energy converters for optimum power capture. IEEE Trans. Sustain. Energy 13 (3), 1869–1872.

Ermakov, A., Ringwood, J.V., 2021. Development of an analytical model for a cyclorotor wave energy device. In: Proceedings of 14th European Wave and Tidal Energy Conference, paper #1885, Plymouth, UK.

Ermakov, A., Ringwood, J.V., 2021a. A control-orientated analytical model for a cyclorotor wave energy device with N hydrofoils. J. Ocean Eng. Mar. Energy 7, 201–210.

Ermakov, A.M., Ringwood, J.V., 2021b. Erratum to: A control-orientated analytical model for a cyclorotor wave energy device with n hydrofoils. J. Ocean Eng. Mar. Energy 7, 493–494.

Ermakov, A., Ringwood, J.V., 2021c. Rotors for wave energy conversion—Practice and possibilities. IET Renew. Power Gener. 15, 3091–3108. http://dx.doi.org/10.1049/rpg2.12192.

Ermakov, A., Ringwood, J.V., 2022. A validated analytical model for a cyclorotor wave energy device. Int. Mar. Energy J. 5 (2), 201–208.

Ermakov, A., Ringwood, J.V., Olbert, G., Arredondo-Galeana, A., Pascal, R., Papillon, L., Thiebaut, F., Grégory, P., 2021. LiftWEC project deliverable D5.2 validated numerical model with real-time computational capabilities. https://liftwec.com/ (accessed 03 February 2023).

Fagley, C.P., Seidel, J.J., Siegel, S.G., 2012. Wave cancellation experiments using a 1:10 scale cycloidal wave energy converter. In: Proceedings of 1st Asian Wave and Tidal Conference Series, Jeju Island, Korea.

Fernandez Chozas, J., Têtu, A., Arredondo-Galeana, A., 2021. A parametric cost model for the initial techno-economic assessment of lift-force based wave energy converters. In: Proceedings of 14th European Wave and Tidal Energy Conference. Plymouth, UK.

Folley, M., Whittaker, T., 2019. Lift-based wave energy converters – an analysis of their potential. In: Proceedings of the 13th European Wave and Tidal Energy Conference. Napoli, Italy.
Gabriel, T., Ignazio, M., 2020. Unsteady hydrodynamics of tidal turbine blades. Renew. Energy 146, 843–855.
Guo, B., Ringwood, J.V., 2021. A review of wave energy technology from a research and commercial perspective. IET Renew. Power Gener. 15 (14), 3065–3090.
Hermans, A., Pinkster, J., 2007. A rotating wing for the generation of energy from waves. In: Proc. 22nd International Workshop on Water Waves and Floating Bodies. pp. 165–168.
Hermans, A., Van Sabben, E., Pinkster, J., 1990. A device to extract energy from water waves. Appl. Ocean Res. 12 (4), 175–179.
Lei, S., Annie-Claude, B.-L., Olivier, C.-D., 2022a. Analysis of flow-induced performance change of cycloidal rotors: Influence of pitching kinematic and chord-to-radius ratio. Ocean Engineering 263, 112382.
Lei, S., Annie-Claude, B.-L., Olivier, C.-D., 2022b. Numerical investigations on unsteady vortical flows and separation-induced transition over a cycloidal rotor at low Reynolds number. Energy Conversion and Management 266, 115812.
2022. LiftWEC consortium. https://liftwec.com/ (accessed 03 February 2023).
Martinez, A., Iglesias, G., 2022. Mapping of the levelised cost of energy for floating offshore wind in the European Atlantic. Renew. Sustain. Energy Rev. 154, 111889.
Olbert, G., 2022. High-Fidelity Modelling of Lift-Based Wave Energy Converters in a Numerical Wave Tank (Ph.D. thesis, Ph.D. thesis). Institute for Fluid Dynamics and Ship Theory, TUHH, Hamburg, Germany.
Olbert, G., Papillon, L., Pascal, R., Ermakov, A., Thibaut, F., 2021. LiftWEC project deliverable D3.3: Tool validation and extension report. https://cordis.europa.eu/project/id/851885 (accessed 03 February 2023).
Penalba, M., Kelly, T., Ringwood, J.V., 2017. Using NEMOH for modelling wave energy converters: A comparative study with WAMIT. In: Proceedings of 12th European Wave and Tidal Energy Conference. Cork., Ireland.
Ringwood, J.V., Ermakov, A., 2022. Energy-maximising control philosophy for a cyclorotor wave energy device. In: 41st International Conference on Ocean, Offshore & Arctic Engineering (OMAE). American Society of Mechanical Engineers, Hamburg.
Scharmann, N., 2018. Ocean Energy Conversion Systems: the Wave Hydro-Mechanical Rotary Energy Converter (Ph.D. thesis, Ph.D. thesis). Institute of Mechanics and Ocean Engineering, TUHH, Hamburg, Germany.
Sheldahl, R., Klimas, P., 1981. Aerodynamic Characteristics of Seven Symmetrical Airfoil Sections Through 180-Degree Angle of Attack for Use in Aerodynamic Analysis of Vertical Axis Wind Turbines. Sandia National Labs., Albuquerque, pp. 22–23.
Siegel, S., 2013. Cycloidal Wave Energy Converter, Final Scientific Report: DOE Grant DE-EE0003635. Federal Agency to which Report is submitted: DOE EERE – Wind and Water Power Program, USA.
Siegel, S., 2014. Wave climate scatter performance of a cycloidal wave energy converter. Appl. Ocean Res. 48, 331–343.
Siegel, S.G., 2019. Numerical benchmarking study of a cycloidal wave energy converter. Renew. Energy 134, 390–405.
Siegel, S., Fagley, C., Nowlin, S., 2012a. Experimental wave termination in a 2D wave tunnel using a cycloidal wave energy converter. Appl. Ocean Res. 38, 92–99.
Siegel, S.G., Fagley, C., Römer, M., McLaughlin, T., 2012b. Experimental investigation of irregular wave cancellation using a cycloidal wave energy converter. In: Proc. Intl. Conf. on Offshore Mechanics and Arctic Eng. (OMAE), Rio de Janeiro, Vol. 44946. American Society of Mechanical Engineers, pp. 309–320.
Têtu, A., Fernandez Chozas, J., 2021. A proposed guidance for the economic assessment of wave energy converters at early development stages. Energies 14 (15).
Thiebaut, F., Payne, G., 2021a. LiftWEC project deliverable D4.4 report on physical modelling of 2D LiftWEC concepts. https://cordis.europa.eu/project/id/851885. (accessed 03 February 2023).
Thiebaut, F., Payne, G., 2021b. LiftWEC project deliverable D4.7 open-access experimental data from 3D LiftWEC tests.
Thiebaut, F., Payne, G., Haquin, S., Weber, M., Lamber, S., Pettinotti, B., 2021. LiftWEC project deliverable D4.3 open access experimental data from 2D scale model. https://doi.org/10.5281/zenodo.5534471 (accessed 03 February 2023).
Wehausen, J., Laitone, E., 1960. Surface Waves, Handbook of Physics, Vol. 9. Springer-Verlag.
Wu, X., Zuo, L., 2022. Preliminary modeling of angle of attack in self-rectifying turbine under high rotational speed. In: Proceedings of the ASME: The 34th Conference on Mechanical Vibration and Sound (VIB).
Yu, C., Andong, L., Xiaochuan, Y., Ziyan, L., Xiaobo, T., Shiming, W., 2021. Experimental tests and CFD simulations of a horizontal wave flow turbine under the joint waves and currents. Ocean Eng. 237, 109480.